SANDIA REPORT

SAND2001-1708
Unlimited Release
Printed June 2001

Meso-Machining Capabilities

Gilbert L. Benavides, David P. Adams, and Pin Yang

Prepared by
Sandia National Laboratories
Albuquerque, New Mexico 87185 and Livermore, California 94550

Sandia is a multiprogram laboratory operated by Sandia Corporation, a Lockheed Martin Company, for the United States Department of Energy under Contract DE-AC04-94AL85000.

Sandia National Laboratories

Issued by Sandia National Laboratories, operated for the United States Department of Energy by Sandia Corporation.

Available to DOE and DOE contractors from
U.S. Department of Energy
Office of Scientific and Technical Information
P.O. Box 62
Oak Ridge, TN 37831

Telephone: (865)576-8401
Facsimile: (865)576-5728
E-Mail: reports@adonis.osti.gov
Online ordering: http://www.doe.gov/bridge

Available to the public from
U.S. Department of Commerce
National Technical Information Service
5285 Port Royal Rd
Springfield, VA 22161

Telephone: (800)553-6847
Facsimile: (703)605-6900
E-Mail: orders@ntis.fedworld.gov
Online order: http://www.ntis.gov/ordering.htm

Issued by Sandia National Laboratories, operated for the United States Department of Energy by Sandia Corporation.

Available to DOE and DOE contractors from
U.S. Department of Energy
Office of Scientific and Technical Information
P.O. Box 62
Oak Ridge, TN 37831

Telephone: (865)576-8401
Facsimile: (865)576-5728
E-Mail: reports@adonis.osti.gov
Online ordering: http://www.doe.gov/bridge

Available to the public from
U.S. Department of Commerce
National Technical Information Service
5285 Port Royal Rd
Springfield, VA 22161

Telephone: (800)553-6847
Facsimile: (703)605-6900
E-Mail: orders@ntis.fedworld.gov
Online order: http://www.ntis.gov/ordering.htm

SAND2001-1708
Unlimited Release
Printed June 2001

Meso-Machining Capabilities

Gilbert L. Benavides, David P. Adams, and Pin Yang

Manufacturing Science and Technology Center
Sandia National Laboratories
P.O. Box 5800
Albuquerque, NM 87185-0958

Abstract

Meso-scale manufacturing processes are bridging the gap between silicon-based MEMS processes and conventional miniature machining. These processes can fabricate two and three-dimensional parts having micron size features in traditional materials such as stainless steels, rare earth magnets, ceramics, and glass. Meso-scale processes that are currently available include, focused ion beam sputtering, micro-milling, micro-turning, excimer laser ablation, femtosecond laser ablation, and micro electro discharge machining. These meso-scale processes employ subtractive machining technologies (i.e., material removal), unlike LIGA, which is an additive meso-scale process. Meso-scale processes have different material capabilities and machining performance specifications. Machining performance specifications of interest include minimum feature size, feature tolerance, feature location accuracy, surface finish, and material removal rate. Sandia National Laboratories is developing meso-scale mechanical components and actuators which require meso-scale parts fabricated in a variety of materials. Subtractive meso-scale manufacturing processes expand the functionality of meso-scale components and complement silicon based MEMS and LIGA technologies.

Acknowledgment

The authors thank and acknowledge the important contributions provided by Merlin Decker, *Advanced & Exploratory Systems dept., Sandia National Labs (SNL),* Jose Gonzales, *Project & Miniature Machining dept., SNL,* John Sullivan, *Nanostructure & Semiconductor Physics dept., SNL,* Kevin Zavadil, *Corrosion Science & Technology dept., SNL,* Barry Ritchey, *Organic Materials dept., SNL,* Bernie Jokiel, *Mechanical Engineering dept., SNL,* Dr. Dennis Alexander, *University of Nebraska,* and Dr. Michael Vasile, *Louisiana Tech University,*

Merlin Decker worked on the development of LIGA fabricated electrodes for the sinker micro Electro Discharge Machine (micro-EDM). Jose Gonzales machined parts using the sinker micro-EDM. John Sullivan and Kevin Zavadil allowed us to salvage their Excimer laser. Barry Ritchey created many of the SEM images used in this report. Bernie Jokiel assembled and programmed the meso-scale stepper motor. Dr. Dennis Alexander provided femtosecond laser machining. Dr. Michael Vasile helped Sandia to obtain a donated focused ion beam machine and taught us how to fabricate micro-tools.

This report serves to summarize the results and satisfies the requirements for the Laboratory Directed Research and Development (LDRD) project “Advanced Machining Processes for Microfabrication”, project number 10353. This LDRD project was funded by the Advanced Manufacturing Investment Area.

Contents

Page

Intentionally Left Blank.

1.0 Introduction

Sandia National Laboratories has a need to machine meso-scale features in a variety of materials. In the past, Sandia has developed precision miniature-scale electro-mechanical components. Presently, Sandia has been developing functionally similar electro-mechanical components using technologies such as silicon based MEMS and LIGA. The authors recognized that there was a void in our ability to fabricate meso-scale parts and features. There is also a need to machine meso-scale features in traditional engineering materials like stainless steels, ceramic, and rare earth magnets. Examples of meso-scale features are, fillets, spherical radii, contours, holes, and channels. Figure 1.1 is an illustration of the relative size of critical dimensions for miniature, meso, and micro machining. In general, meso-machining processes should be capable of machining feature sizes of 25 microns or less. Unlike LIGA which is an additive technology, the meso-machining technologies that are being developed are subtractive in that material is removed to fabricate a part. These subtractive technologies are, focused ion beam machining, micro-milling, micro-turning, laser machining, and micro electro-discharge machining. Sandia is driven to develop micro- and meso-scale fabrication technologies to meet the needs of the nuclear weapons stockpile.

The focused ion beam (FIB) machines metals by bombarding the work piece with a nanometer scale diameter beam of gallium ions. The material removal rate for focused ion beam machining is very low, on the order of 0.5 cubic microns per second. Given the low material removal rate, the effort is placed upon fabricating tools that can be used repetitively to remove material at much faster rates. Examples of these tools are 25 micron diameter end mills, masks for photolithography and masks for laser machining. Sandia has successfully milled square channels having a cross section of 25 microns by 25 microns in PMMA, aluminum, brass, and 4340 steel using a high precision milling machine. The work related to using the FIB to fabricate hard tooling, has been a joint effort between Sandia National Laboratories and Louisiana Tech University.

The two laser machining processes that are being developed are nanosecond excimer ablation and femtosecond Ti-sapphire ablation. The excimer laser, which has a pulse width on the order of nanoseconds, can readily machine meso-scale holes and channels in polymers and ceramics. A mask projection technique can be introduced in the expanded portion of the excimer laser beam to project a complex de-magnified replica of the mask onto the workpiece. The femtosecond Ti-sapphire laser can readily machine micro-scale holes and channels in metals. The femtoscond laser machining process can fabricate a one micron diameter, high aspect ratio hole in metal with minimal debris. Laser machining can be used to create three dimensional features because depth of cut is very well correlated to exposure time.

Sandia has both sinker and wire micro Electro Discharge Machining (micro-EDM) capabilities. Sandia only recently took possession of the Agie wire micro-EDM and therefore we did not have any results available for this publication. Sandia's Agie Compact 1 micro-sinker electro-discharge machine (EDM) is being used to machine features as small as 25 microns in difficult materials such as stainless steels and kovar. This class of EDM technology employs a micro-generator that is capable of controlling over-burn gaps to as little as three microns. LIGA

technology is being employed to fabricate small intricate copper electrodes. These are mounted to the micro-sinker EDM to machine the complementary shape into these difficult materials.

These subtractive meso-scale machining technologies generate issues in regards to cleanliness, assembly, and tribology. Some issues are unique to meso-scale machining while other issues can be regarded as an extension of similar macro-scale issues. Cleanliness is important because meso-scale critical dimensions can easily be exceeded by dirt particle size or debris created during the machining process. Meso-scale milling and turning can create chips and burrs that can block holes or create a mechanical interference. Surface morphology and surface finish conditions vary greatly depending upon the meso-scale machining technology. The great variety of materials and surface conditions create a complex parameter set for characterizing tribological phenomenon. Meso-scale parts are difficult to handle and align which makes assembly a challenge.

Other issues exasperated at the meso-scale are material stability and bearing considerations. Some materials are dimensionally unstable and change shape after machining due to the relaxation of the material or the action of tooling forces imparted during the machining process. Low aspect ratio parts may be especially vulnerable to warpage. A list of stable materials is being compiled at Sandia National Laboratories. Meso-scale parts that require relative motion create a unique challenge in regard to low friction bearings. Often times conventional ball bearings are not an option. The solution may be the resurrection of an old and dying technology known as jeweled bearings.

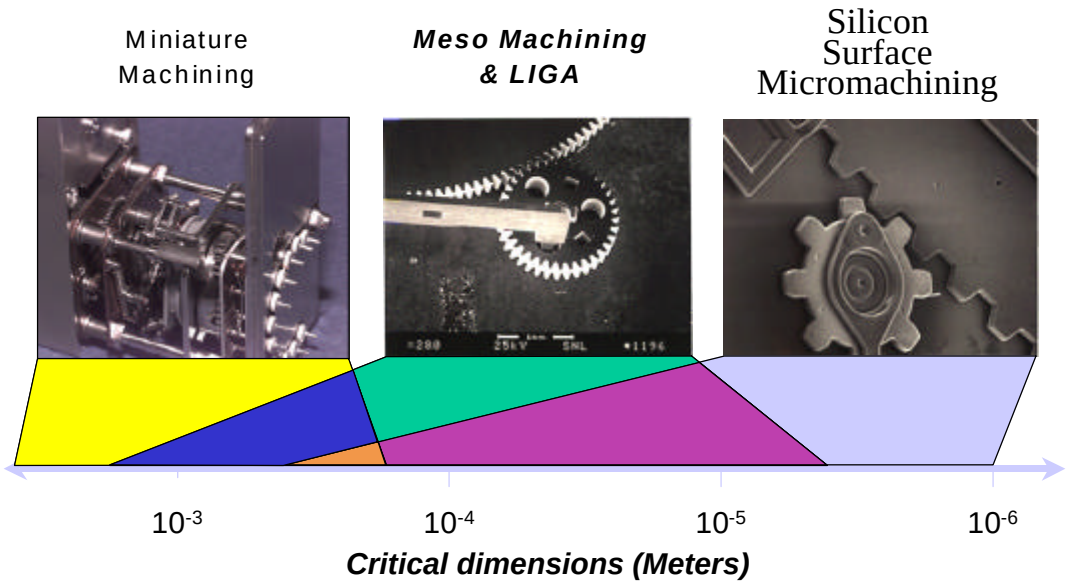

Figure 1.1: Perspective of miniature machining, meso-machining, and micro-machining (figure provided by David Plummer, SNL).

2.0 Focused Ion Beam sputtering and Microtool machining

In this work focused ion beam (FIB) sputtering is combined with ultra-precision machining for microfabrication. Ion sputtering is used to shape micro-cutting tools that are capable of milling or turning complex features in a host of materials. This includes creation of features on nonplanar workpieces.

Ultra-precision machining techniques are attractive for patterning complex features on a variety of workpiece geometries and materials. In general, control of micron feature sizes is made possible by computer numerically controlled (CNC) ultra-precision machines. Commercial instruments have 5-nm positional accuracy in different directions and specially designed tool holders that minimize error. CNC ultra-precision machines have been used by many groups to create miniature components while maintaining sub-μm tolerances. Despite the high precision of these instruments, there is a need for smaller cutting tools. Based on a search of tool manufacturers, we find that the smallest commercially available milling tools[1] are ~125 μm in diameter. Research continues to develop new microtool fabrication techniques. For example, Vasile et. al. first demonstrated the use of focused beams for shaping microtools.[2]

In this work we research and develop techniques for shaping robust, micro-cutting tools. FIB sputtering is chosen to fabricate microtools, because this technique affords precise control over feature size, permits a variety of tool geometries and establishes sharp cutting edges. A focused ion beam is typically less than 0.5 μm in diameter, allowing for small features with sub-μm tolerances. Also, stages can position tools with sub-μm accuracy and rotate these over a large range of angles. Therefore, multiple nonplanar facets can be created to establish tool clearance, rake or taper. FIB sputtering applied to tool fabrication is well controlled due to precise beam positioning and dose allocation. Ion sources, focusing optics and beam deflectors are extremely stable over many hours. Furthermore, microtool fabrication is reproducible, because ion sputtering is a relatively 'stress-free' process. Compared with techniques such as mechanical grinding, there is less force on a tool during fabrication.

Two types of microtools are fabricated in this study: micromilling tools and micro-turning tools. Micromilling is an ultra-precision technique that shows promise of machining features down to micron length scales in planar workpieces. Micro-turning is used to fabricate small features in cylindrical workpieces.

2.2 Description of focused ion beam system

Microtools are shaped using a custom-made focused ion beam system, described in detail elsewhere.[3] As shown in Figure 2.1., the FIB system consists of a liquid metal ion source, beam deflectors, sample stage, and channelplate detector for secondary electron imaging. The ion gun produces a 20 keV beam of Ga^+ ions with a near-Gaussian intensity distribution and a full-width at half-maximum diameter of 0.4 μm. Currents are typically 2 nA in a Faraday cup giving a current density of ~ 1.5 A/cm^2. The Ga^+ source chamber is ion pumped and has a pressure of 10^{-9} Torr. The target chamber uses an oil diffusion pump to maintain a pressure of

10^{-8} Torr during sputtering. A small aperture separates the two chambers for efficient differential pumping. A load lock chamber is attached to the vacuum system. This preserves the high vacuum in the target chamber and allows for rapid sample exchange. A sample cassette is used to hold tool blanks. It provides for sample rotation with a minimum step size of 0.37^{o} per pulse. The cassette is clamped onto a vacuum stage that positions samples with 1μm absolute accuracy.

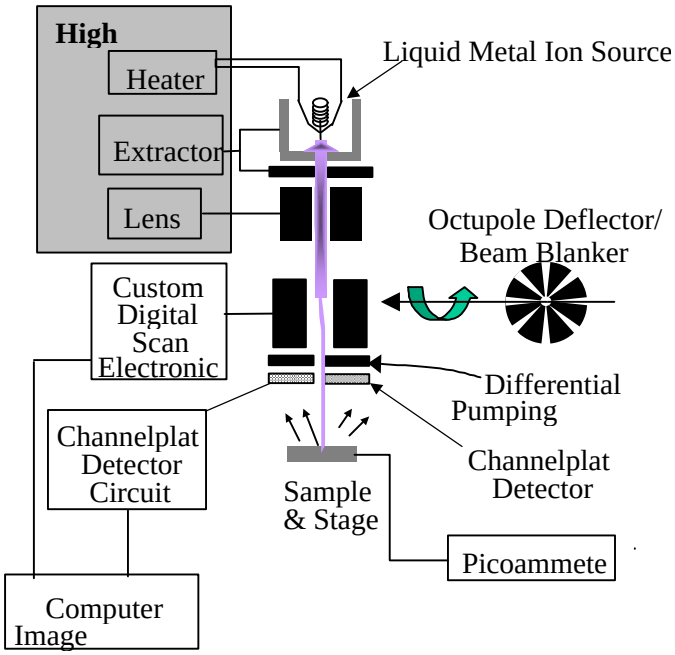

Figure 2.1. Schematic of focused ion beam

In practice, an operator outlines a desired shape on a secondary electron image, and an octupole deflection system steers the ion beam over desired areas with sub-μm resolution. A variety of shapes are possible with existing software including polygons. Additional software allows an operator to mill predetermined curved shapes, such as sinusoids, paraboloids and hemispheres into samples. This is accomplished by correctly allocating ion dose to each pixel and compensating for the variation in sputter yield with incidence angle.

2.3 Basics of microtool sputter fabrication technique

We shape microtools by ion beam sputtering a number of critically-aligned facets. With the FIB stage and tool fixed, the gallium beam impinges normal to a plane containing the tool axis as shown in Figure 2.2. This ion-solid geometry is chosen, because it produces one edge per facet that is sufficiently sharp for cutting. Previous work by Vasile et. al.[4] shows that the edge of a facet closest to the ion source is rounded having a radius of curvature of ~ 1.0 μm. This rounding arises due to the Gaussian intensity of the beam; although a pattern boundary is defined for ion beam milling by the operator, the tails of the intensity distribution extend outside of this boundary leading to a curved surface. Nevertheless,

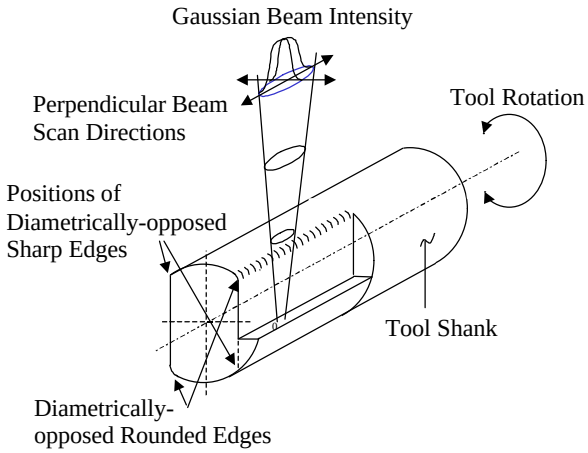

Figure 2.2. Geometry used for defining facets on micro-milling tools

continued ion beam sputtering with this particular geometry makes the edge furthest from the ion source sharp. A sharp edge having a radius of curvature < 0.1 μm is produced, because the ion beam has a truncated intensity distribution tail at the far side of a facet due to shadowing by the tool. We designated these sharper edges as microtool cutting edges.

As shown in Figure 2.2. for a micromilling tool, ion beam sputtering is used to make face cuts on a tool blank. We avoid making spiral flutes for several reasons. Three-dimensional micromachining of curved surfaces is complicated by a variation in sputter yield with the ion/solid angle of incidence.[5] A spiral flute requires a distribution of angled features, thus complicating tool fabrication. Also, tool rigidity is required for cutting, and we desire to minimize fabrication time. In general, a small amount of material is removed. Milling tools are fabricated in ~ 2 hours depending on the design. Threading tools are shaped in approximately 6 hours.

Multiple facets are made by rotating a tool to different orientations with respect to the beam. Rotation of a tool between sputtering steps allows control of tool geometry and clearance behind cutting edges.

2.4. Milling tools: Design and Fabrication

Focused ion beam (FIB) sputtering is used to shape a variety of micro-end mill tools. Precise fabrication of microtools allows for a meaningful comparison of tool diameter with micromachined feature width for different machining parameters.

Micro-end mill tool blanks are purchased from National Jet, Inc. and are made of materials commonly used for machine tools. This includes cobalt M42 high-speed steel or C2 micrograin tungsten carbide. Tool shanks are 1.02 mm in diameter and are brazed into a centerless ground mandrel. One end of each shank is tapered by diamond grinding and polished; this end has a 25 μm diameter and is cylindrical over a length of 90 μm.

A micro-end mill is shaped from a polished tool blank by ion sputtering a number of nonplanar facets as shown in Figure 2.3. The end of a tool blank is first bombarded (not shown) to remove approximately 5 μm from the 90 μm long, ~25 μm diameter cylindrical portion. This creates a polished facet with a

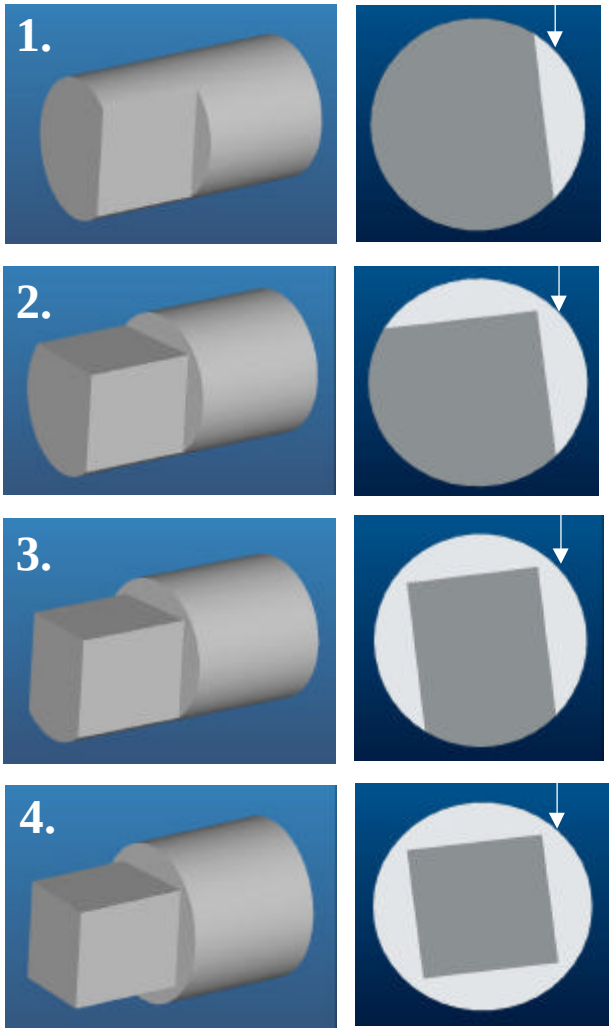

Figure 2.3. Schematic of micro-end mill fabrication process

normal direction oriented 7° with respect to the tool axis. This tool-end facet is intended to provide clearance for chip removal during mechanical milling. After modifying the tool end, the ion beam is deflected over areas approximately 3 μm by 50-75 μm to create chip-cutting facets. With the FIB stage and tool fixed, the gallium beam impinges normal to a plane containing the tool axis, but tangential to the tool circumference. As described in the previous section, this ion-solid geometry is chosen, because it produces one extremely sharp edge per facet. An SEM image showing a sub-μm radius of curvature is presented in Figure 2.4.

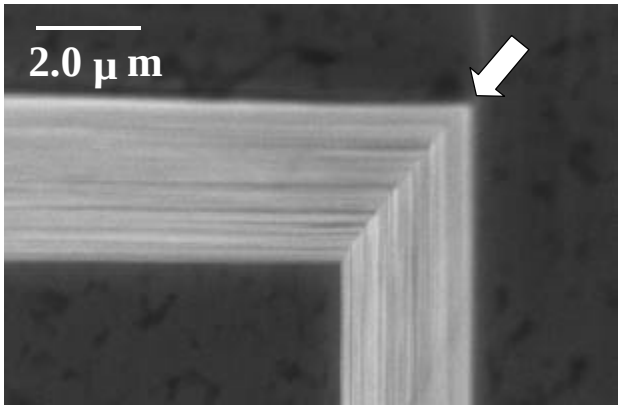

Figure 2.4. Sharp cutting edge on tungsten carbide, four-side micro-end mill.

Numerous facets can be formed by sequentially rotating tools and sputtering. The number and position of facets on a micro-end mill uniquely determine the properties of a tool, such as clearance for removing a chip and tool rotation direction for milling. Figure 2.5. shows micro-end mills having 2, 4 and 6 cutting facets made by focused ion beam sputtering. The tool in Figure 2.5.a. has two cutting facets and two diametrically opposed sharp edges. Figure 2.5.c. shows a tool having six cutting facets and clearance behind each of the five cutting edges, since almost the entire circumference is sputtered. In this study six-facet end mill tools are made with 4, 5 or 6 sharp edges by selecting a particular stage rotation sequence between sputter steps. The placement of facets by FIB sputtering determines tool rotation direction for milling

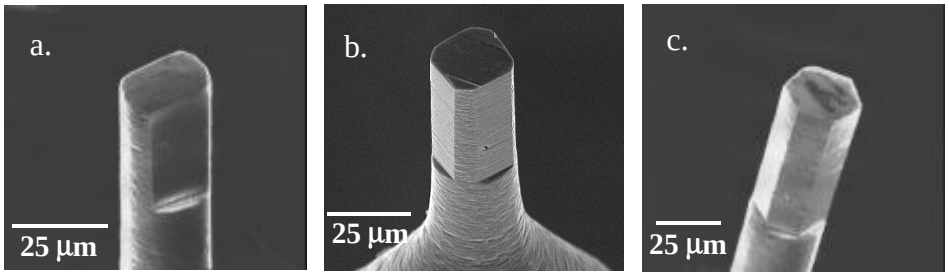

Figure 2.5. Micromilling tools shaped by focused ion beam sputtering.

operations. Micro-end mills have been made so that sharp facet edges cut while rotating the

tool clockwise or counter-clockwise. Note, only tools made for a clockwise rotation (looking down on a workpiece) are tested.

Micromilling tools are fabricated in 2-3 hours depending on design and tool material. In general, a tool having a large number of facets is fabricated in a relatively short time, because less material is removed. For example, the time required to make the six-facet tool shown in Figure 2.5.c. is less than the time needed for the other tools shown. The fabrication time depends on tool material, since sputter rate is a function of the target mass. The sputter rate for tungsten carbide is quantified by bombarding polished wafers of identical C2-grade material with a fixed gallium dose equal to 1.0×10^{19} ions/cm^2 (i= 2.8 nA) at 20keV. Areas 20 μm x 20μm are sputtered to a small depth in order to avoid re-deposition, using a 72 μsec pixel dwell time, a 0.19 μm pixel spacing and a 0.86 sec refresh time. A single near-normal angle of incidence is used for this control experiment. Afterwards, a portion of the feature is cross-sectioned with the gallium beam, and the depth is measured away from the feature edges. Average depth is measured by tilting the sample to a known angle in the scanning electron microscope and taking several measurements along the feature bottom boundary. Using the sputtered volume, an average rate of removal is calculated to be 0.76 μm^3/sec.

When using FIB sputtering to fabricate microtools, it is important to note that each facet forms an angle of ~7^o with respect to the incident ion beam direction. (See Figure 2.3.) This occurs because of minimal sputter yield at incidence angles greater than 83^o with respect to the surface normal.[6] Ions impinging on a surface at near-glancing angles most often reflect without displacing atoms from lattice sites. However, tools can be aligned with respect to the beam direction in order to compensate for this sputter-induced angle.

2.5. Micromilling tools: Tests

Two high precision milling machines are used to test focused ion beam-fabricated tools and to develop machining procedures. This includes a Boston Digital mill and a modified National Jet 7M milling instrument.[7] The Boston Digital apparatus has 1.0 μm resolution in the plane of the workpiece (x and y) and 0.5 μm depth resolution. Tools are held in a collet to minimize error. The National Jet 7M instrument has a 1500 kg granite machine base for vibrational and thermal stability, and all axes have air bearings. In addition, the x and y motions of the work table employ laser interferometry with a commanded resolution of 1.25 nm, and the z motion has linear encoder positional control with a resolution of 20 nm. All travel ranges are 150 mm. The micromilling head consists of a specially designed v-block bearing arrangement having four spherically convex diamonds. Tools rotate about an axis dictated by the contact positions of the four diamond surfaces on the mandrel resulting in a cumulative radial error less than 1 μm. The small error is attributed to variations in tool mandrel surface roughness. All micromachining tests involve a lubricant unless specified. Workpieces are flushed continuously during micromilling with a water-based, sulfur free liquid (Blasser 4000). All milling operations, including registry, are monitored with an optical microscope and CCD camera.

Scanning electron microscopy (SEM) and optical interferometry are used to analyze microtools and machined workpieces. A calibrated JEOL 6300V scanning electron microscope

is used to measure tool diameter, tool edge radius of curvature, trench widths and taper angles. This instrument is calibrated to a NIST/NBS standard (reference # 484 c) and shows less than 2 % error for different working distances (i.e., bottom of pole piece to sample surface). An overall accuracy of 95 % or better is estimated for dimensions measured by SEM. Trench widths are measured from SEM images that view normal to the plane of a workpiece. Additional images that show perspective views are not used for measurement. PMMA samples are coated with ~ 20 nm of Au/Pt to prevent charging in the SEM. A calibrated WYKO (RST^{+}) white light optical interferometric roughness step tester determines the roughness in the bottom of machined trenches. Several regions within the bottom of each micromachined trench are probed to obtain an accurate measurement of lateral and longitudinal surface roughness. A typical measured region is 100 μm long. PMMA samples coated with 20 nm of Au/Pt have a reflective surface for inspection. The step height standard for the roughness step tester is a 23.33 μm metal film (VLSI Standards, Inc.). The phase shift interference resolution of the RST^{+} is 0.3 nm.

Machining at feed rates of 2-3 mm/minute

In the present work micro-end mill tools are tested by milling materials having different degrees of machinability. Initial tests of micro-end mills involve machining at low feed rates, 2 or 3 mm/minute, with an axial depth per pass $\geq$ 0.5 μm. These depths/pass are chosen, because a microtool 'appears' sharp when compared to the cutting action, i.e., the tool edge R_c is less than the thickness removed. Microtools are rotated clockwise in this study so that sharp facet edges cut a workpiece.

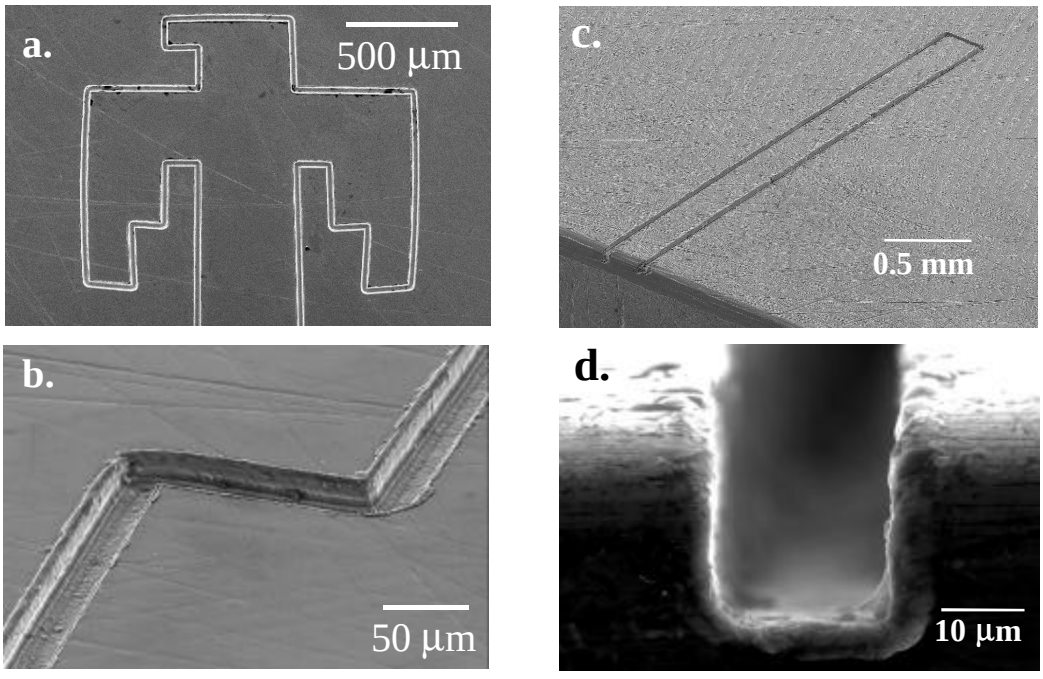

Figure 2.6. Micromilled metal workpieces including brass (a. and b.) and 6061 Al alloy (c. and d.)

FIB-fabricated microtools successfully machine trenches in PMMA, aluminum, brass and 4340 steel [8] at low feed rates. For all tests except for one, 15-25 μm deep trenches are cut several millimeters in length as commanded. Examples of micromachined metal workpieces are shown in Figure 2.6. This includes experiments on brass and 6061-T4 aluminum alloy. As summarized in Table 1.2, the surface roughness (R_a) of most trenches machined at low feed rates is small, ~200 nm or less. In addition, all trenches milled in PMMA, Al alloy and 4340 steel have nearly vertical sidewalls. Near-vertical sidewalls are present on both sides of micromachined trenches as demonstrated in 6061 Al (Figure 2.6.d.). Electron microscopy shows a slight taper of ~1-2^o from vertical. SEM shows that micromachined trench widths are similar to the intended sizes (i.e., tool diameters). Experiments with the Boston Digital apparatus produce trench widths that are ~2 μm larger than the tool diameters. Close matching is found for the different tool designs and workpiece materials. The small deviation from the intended width is attributed to the radial error of the tool and spindle. The combination of tool form error and spindle motion radial error is measured to be 2 μm or less prior to each machining test. Error is probed approximately 2 mm from the end of the mandrel closest to the tool shank using a test indicator. Additional milling tests with the modified National Jet apparatus at large axial depths of cut and rotation speeds to 20,000 rpm produce similar matching. Trenches milled in PMMA are limited at 2 μm larger than the tool diameter. With the National Jet instrument, a tool is held in a v-block bearing assembly that is specially designed to minimize radial error beyond the variations in surface roughness of the tool mandrel. Therefore, we expect that the difference between the micro-end mill diameter and the trench width results from the eccentricity of tool cutting edges and tool vibration. In general, tests with both milling instruments produce trench widths that are uniform over several millimeters. An example of this is shown in Figure 2.6.a. and b. The feature in brass requires 25 passes for completion and demonstrates the positioning repeatability of ultra-precision milling instruments. Note that the curved portions of the micromachined trench, as seen in the SEM micrograph, are part of the intended design and are not image artifacts.

The experiments listed in Tables 2.1. show a single test that results in a significantly larger trench width and surface roughness. This involved tool ‘B2’, a two facet high speed steel micro-end mill. Machining 6061 aluminum at a feed rate of 2 mm/ minute without a lubricant produces a trench width approximately 6.4 μm larger than the tool diameter. Also, the roughness of the trench bottom is measured using optical interferometry to be ~458 nm. It is expected that the lack of a lubricant is responsible for the poor characteristics of this micromachined feature. Note, this ultra-precision machining test resulted in microtool fracture, with breakage occuring during the twenty-second pass. It is estimated that tool B2 is rotated 3.4×10^6 times while in contact with the workpiece prior to fracture. At the time of tool fracture, approximately 6.0×10^6 μm^3 of material had been removed.

There are several indications from the experiments at low feed rates that microtools cut chips rather than remove material by burnishing. In separate experiments on PMMA and 6061 Al, we turn off the lubricant and blow dry the workpiece for brief amounts of time to observe cutting through an optical microscope. Repeatedly there is evidence of small chips being ejected from the vicinity of a moving tool. After rinsing workpieces, trenches are inspected

with SEM to determine the morphology of the bottom surface. In all cases, tool-cutting marks are revealed. Marks are found in micromachined brass, PMMA, Al alloy and steel.

Tool #, #Cutting edges Tool Material	Tool Diameter (μm)	Workpiece Material	Rotation Speed, (rpm)	Feed Rate, (mm/min)	Depth Per pass, (μm)	Mean Trench Width, Standard Deviation (μm)	Roughness, Bottom R_a (nm)
Q2, 4, HSS	24.0	PMMA	18,000	2.0	0.5	26.2, 1.5	93
H4, 4, HSS	26.2	Al 6061-T4	10,000	2.0	1.0	28.2, 1.1	92
B2, 2, HSS†	23.6	Al 6061-T4	18,000	2.0	0.5	30.0, 2.0	458
B3, 2, WC	21.7	Al 6061-T4	18,000	3.0	1.0	23.0, 1.1	117
H6, 5, HSS	25.0	Brass	10,000	2.0	1.0	28.8, 0.7	139
Q6, 4, WC	22.5	4340 Steel	18,000	3.0	1.0	23.5, 1.0	162

Tool Code: H = Hex-tool (6 facets); B = Bi-tool (2 facets); Q = Quad-tool (4 facets)
HSS = High Speed Steel; WC = tungsten carbide † *No lubricant used during machining.*

Table 2.1. Machining parameters and results from micromilling different materials at a feed rate of 2 or 3 mm/minute. Boston Digital apparatus is used.

Machining at feed rates of 3-50 mm/minute

Additional ultra-precision machining experiments are used to evaluate microtool performance for increased chip load rates.[9] Milling tests involve constant table feed rates of 3, 10, 25 and 50 mm/minute, and again a tool is rotated clockwise (looking down on the workpiece) so that sharp facet edges cut. A rotation speed of 18,000 rpm is used for each test, and the axial depth per pass is equal to 1.0 μm. For each feed rate, a single two-facet microtool mills 25 μm deep, 7 mm long trenches in 6061-T4 Al. The tool is made of C2 tungsten carbide and has a diameter of 21.7 μm.

As described in Table 2.2., micromilled trench widths are approximately the same size as the tool diameter. Average trench widths range from 22.0 to 23.1 μm. The standard deviation taken from these measurements is also included in the table. In addition, surface roughness measured in the bottom of milled trenches is approximately 200 nm or less, and there is no degradation with increased table feed rate. The morphology in the bottom is characterized by tool cutting marks. The sidewalls of this and other micromachined trenches are nearly vertical. In summary, micromilling tests at higher feed rates suggest that FIB-fabricated microtools mill metal alloys without significant tool dulling. Repeated testing indicates that FIB-fabricated tools are robust despite their small size and 'apparent' delicate nature. The two-facet microtool, labeled 'B3' in Table 2.2., milled 6061 Al for over 6 hours without tool fracture. For a feed rate of 50 mm/ min, aluminum alloy is machined at 18,740 μm^3/sec.

Tool #, # edges, Tool Material	Tool Diameter (μm)	Workpiece Material	Rotation Speed, (rpm)	Feed Rate, (mm/min)	Depth per pass, (μm)	Mean Trench Width, Standard Deviation (μm)	Roughness, Trench R_a (nm)
B3, 2, WC	21.7	Al 6061-T4	18,000	*3.0*	1.0	23.0, 1.1	117
B3, 2, WC	21.7	Al 6061-T4	18,000	*10.0*	1.0	22.0, 0.6	83
B3, 2, WC	21.7	Al 6061-T4	18,000	*25.0*	1.0	23.1, 0.6	82
B3, 2, WC	21.7	Al 6061-T4	18,000	*50*	1.0	22.5, 0.5	102

Tool # Code: 1st letter designates overall shape; B = Bi-tool (2 facets)
Tool Material Code: WC = tungsten carbide

Table 2.2. Machining parameters and results from micromilling Al 6061-T4 at different feed rates including 3, 10, 25 and 50 mm /minute.

2.6 Microthreading/grooving tools: Design and Fabrication

Microthreading/grooving tools are fabricated from tool blanks made of cobalt M42 high-speed steel (HSS), C2 micrograin tungsten carbide or single crystal diamond. Tool shanks made of WC or HSS have a diameter of 1.02 mm and are brazed into a centerless ground mandrel. Tool mandrels are either 2.3 mm or 3.175 mm in diameter. One end of each tool is tapered by diamond grinding and polished; this end has a diameter of approximately 25 μm and is cylindrical over a length of 25 μm.

Microgrooving/threading tools have designs similar to conventional lathe cutting tools, however, cutting edge widths are in the ~10-30 micron range. Each microtool is fabricated from a polished blank to have sharp cutting edges, clearance behind cutting edges and rake features. This is achieved by sputtering a number of strategically placed facets on cylindrical or conical sections at the end of a tool blank as shown in Figure 2.7. In general, the tool rotation/sputter sequence and the location of facets are critical for defining tool characteristics (rake, etc.). The first step of fabricating all micro-grooving and micro-threading tools involves shortening polished blanks. A smooth facet is sputtered at the tool end. After sputtering, the end facet normal is nearly aligned with the tool axis. Next, two facets are created on opposite sides of a tool. This sputter step determines the cutting width, tool cross-section and, hence, the intended cross-sectional shape of a micromachined groove. For example, ion milling two nearly-parallel facets creates a tool

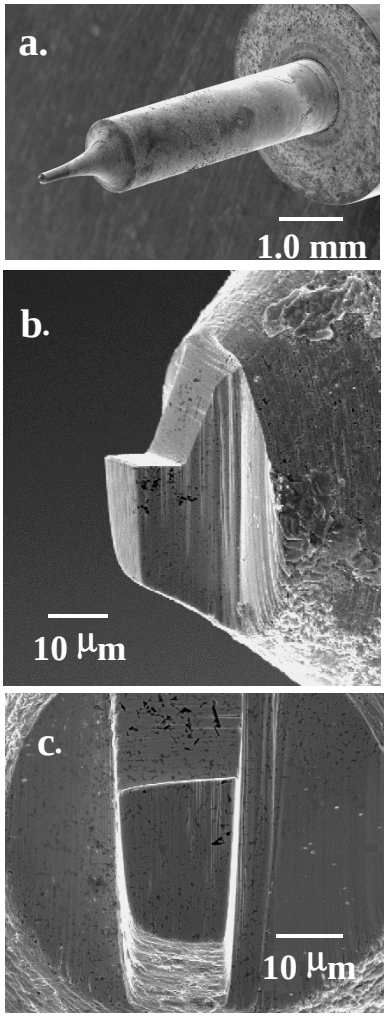

Figure 2.7 Micro-grooving/threading tool made of tungsten carbide. Tool has rectangular cross-section with an 18μm wide tool end cutting edge.

with a rectangular cutting shape. Alternatively a threading tool that cuts trapezoidal cross-section grooves is fabricated by ion milling two nonparallel facets. Sputtering side facets with the geometry described is also critical for establishing taper. Taper provides clearance behind side facet cutting edges thus minimizing contact with workpieces and reducing frictional drag on a tool. During sputtering, each side facet forms a natural taper angle of ~ 5-10^{o} with respect to the ion beam direction as for the milling tools.

After creating side facets, the focused ion beam is used to define rake features that clear chips during ultra-precision machining. First, each tool is rotated -90^{o}in the FIB system. This orients one side facet away from the ion source and places the second side facet such that it nearly faces the source. A triangular projected area is then ion milled on one side of a tool to define a desired back rake angle. The FIB system can accurately define this angle with a resolution of 0.25^{o}. In this study, micro-grooving tools are made with a back rake angle between 0 and 10^{o}, referenced to the tool axis. Tools are made to have a 0^{o} back rake angle in order to increase rigidity. FIB sputtering is also used during this step to set the rake facet length, typically 10-20 μm. Note, a natural taper angle of ~ 5-10^{o} with respect to the ion beam direction accompanies rake feature definition, independent of the back rake angle chosen. This taper can be used to establish side rake, displayed in an end-on view of a tool, Figure 2.7.c. The side rake angle can be changed or eliminated, i.e., forced to 0^{o}, by proper rotation of the stage / tool prior to ion milling this facet.

A sharp cutting edge having clearance is created at the microtool end as a final step of fabrication. Tools are first rotated to their original orientation with respect to the ion beam, and the length is reduced approximately 3 μm by sputtering. This creates an end facet that intersects the rake facet at a well-defined, sharp edge. Measurements from SEM show this edge has a radius of curvature (R_c) of 0.4 μm or less. Radii are measured by viewing parallel to the cutting edge. In addition to creating a sharp edge for cutting, this ion milling step establishes clearance. A taper angle of ~ 5-10^{o} behind the tool end cutting edge prevents unnecessary contact with workpieces.

The microtool fabrication technique described is one variant that can be modified to make tools with different cross-sectional shapes, including semicircular or trapezoidal. A different FIB-fabricated threading/grooving tool is shown in Figure 2.8. This tool is similar in size to the

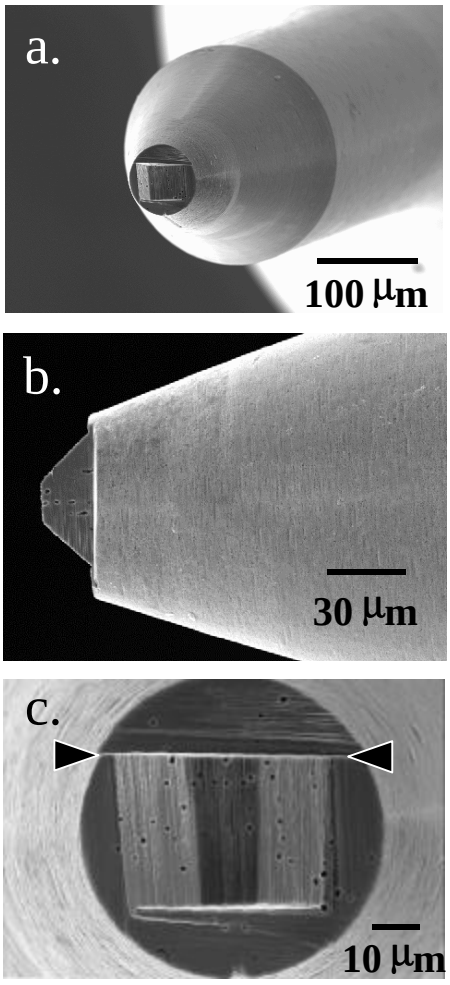

Figure 2.8. High speed steel tool having a trapezoidal cross-section.

microtool shown in Figure 2.7.; however, this has a trapezoidal cross-section and 0^o rake angles. The images in Figure 2.8. show three cutting edges, similar to a stub-threading tool. The side facet cutting edges are oriented 90^o apart, and the leading edge of the tool is 15 μm wide. The taper behind cutting edges is displayed in a secondary electron micrograph of the tool end, Figure 2.8.c.

The small but detectable roughness of cutting facets is due to ion beam sputtering. Most likely, the compositional inhomogeneity of tungsten carbide and high speed steel affects the smoothness. Track marks can develop along facets during sputtering because of shadowing by second phase particles (or other compositional variations) within a tool. For example, cobalt is present in C2-grade tungsten carbide and has a different sputter yield compared with the matrix. Fabricated microtools are polycrystalline with grains oriented in different directions. Track marks and compositional variations within C2 tungsten carbide are seen in Figure 2.7.b. and c. In these SEM micrographs, regions that have a low electron yield appear dark. Energy-dispersive x-ray spectroscopy reveals that the low yield features in Figure 2.7. are Co–rich and C-rich regions. We expect that sharper tool cutting edges can be achieved by focused ion beam sputtering of other tool materials. Single crystal materials (e.g., diamond) should exhibit minimal variation in sputter yield from point to point due to compositional uniformity.

2.7 Microthreading/grooving tools: Tests

This section describes a number of experiments that test the performance of focused ion beam fabricated microtools. Tests involve machining helical features in polymer, ceramic and metal workpieces.

Ultra-precision turning involves a Precitech Optimum 2000 high precision lathe (Louisiana Tech University, courtesy of Professor Michael Vasile). The Precitech lathe operates with both the x and z axis drive mechanisms mounted on a granite platform lapped co-planar to 1.3 μm and isolated from the machine frame to prevent unwanted vibrations. Identical fully-constrained, dovetail-type air bearing slides provide smooth motion for the two axes with less than 0.25 μm deviation per 102 mm of motion. The total length of travel is 191 mm and the maximum slide speed is 1000 mm/min. The two slides are oriented perpendicular to within 2 arc-seconds. Linear laser holographic scales and read-head assemblies provide stable positional feedback for both axes with 8.6 nm resolution. The spindle is supported by fully pre-loaded, high stiffness air bearings and is driven by an integrally mounted brushless DC motor and encoder with range from 0 to 5000 rpm. In order to accurately ‘touch-off’, operations are monitored with an optical microscope and CCD camera. Water continuously flushes workpieces during ultra-precision machining. After machining, workpieces are rinsed with isopropyl alcohol. However, in this study burrs are not removed by mechanical or electrochemical polishing.

Microthreading tools and certain micromachined workpieces are analyzed by scanning electron microscopy (SEM). An overall accuracy of 95 % or better is estimated for dimensions measured by an Amray 1830 scanning electron microscope. This microscope is calibrated to a NIST SRM 2090 standard in the 100 μm range and shows a –2.4 % to –2.6 % error when

using a fixed working distance (i.e., bottom of pole piece to sample surface). In addition, a calibrated JEOL 6300V scanning electron microscope is used to measure widths of grooves machined in cylindrical workpieces. This instrument is calibrated to a NIST/NBS standard (reference # 484 c) and shows less than 2 % error for different working distances. The widths of grooves machined in cylindrical workpieces are determined by viewing feature cross-section.

FIB-fabricated, micro-grooving/threading tools are tested by machining helical grooves in different cylindrical workpieces.[10] A polished, cylindrical workpiece is mounted into a pin vice concentric with the lathe axis of rotation, and a tool holder post is arranged perpendicular. The workpiece is first polished to run true on the lathe, using a diamond bit; this establishes a workpiece surface finish of approximately 1μm (rms) or better. Afterwards, a FIB-fabricated microtool is loaded and aligned with its axis perpendicular to the workpiece axis. Using a scribe mark on the mandrel for alignment, the tool is then rotated to an orientation such that the tool-end cutting edge is nearly parallel to the workpiece axis. An alignment accuracy of tool cutting edges to better than 0.5^{o} ensures minimal contact of side facets with the groove wall. The microtool is then stepped toward the rotating workpiece and registered. Once the workpiece is contacted, the tool is driven into the workpiece to a targeted groove depth and linear motion is initiated.

Using this technique, micro-grooving tools cut helical grooves into cylindrical samples made of 6061-T6 aluminum alloy. Figure 2.9.a. shows a portion of a 13.2 μm wide, 4 μm deep groove having a total length of 200 mm. The pitch between successive passes is 100 μm and is set by the relative rotation rate and the axial feed rate. A change in pitch can be achieved by simply increasing/decreasing these rates. Electron microscopy demonstrates a close match of tool size and micromachined feature width. Measurements show that the groove width is approximately the same as the cutting edge width, 13.0 μm, over the length of the feature. Also, high magnification images demonstrate close matching of tool shape and feature cross-section. SEM analysis of the micromachined groove bottom shows a 6^{o} taper with respect to the cylinder axis. This is identical to the angle of the tool-end cutting edge.

A precise matching of tool shape and groove cross-section also results from machining polymeric cylindrical workpieces. Figure 2.9.b. shows portions of a groove cut in 1.38 mm diameter PMMA. The pitch is 50 μm and the total groove length is 420 mm. The total time to cut PMMA is approximately 30 seconds.

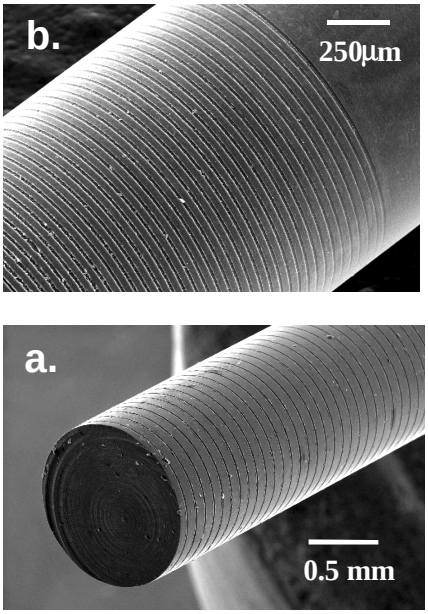

Figure 2.9. Cylindrical workpieces machined with lathe microtool. Helical grooves are fabricated into (a.) Al 6061 and (b.) PMMA.

SEM measurements show that the micromachined groove is consistently 13.1 μm wide over the entire cylinder length, and nearly the same as the tool width, 13.0 μm. In addition, SEM indicates a uniform 6^{o} taper throughout the groove bottom, closely matching the shape of the tool end. Optical interferometry indicates that the roughness in the bottom of machined grooves remains small, similar to that for aluminum. By analyzing a number of line scans across the micromachined groove, the average rms roughness is measured to be 0.25 μm. Analysis of microtools immediately after machining cylindrical workpieces reveals that chips are cut and raked away from workpiece surfaces. An indication of this is shown in Figure 2.10.a. which displays a long PMMA chip wrapped around the shank of a microtool. The chip width is approximately equal to the cutting edge width. Additional SEM at higher magnification indicates chip raking. Figure 2.10.b. shows aluminum chips deflected by a rake facet with minimal accumulation behind the tool-end cutting edge.

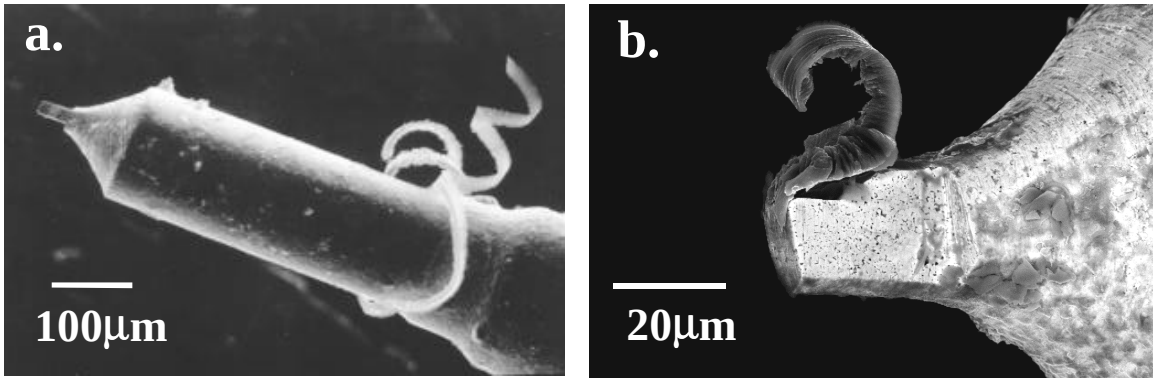

Figure 2.10. Scanning electron micrographs of micro-grooving tools after machining PMMA (a.) and 6061-T6 aluminum (b.).

The techniques used for making micro-end mills and microthreading tools are capable of fabricating even smaller tools. Beam sizes for the FIB system are 0.4 μm, and positioning resolution is better than 1 μm. Tools made to smaller dimensions must have suitable microstructures that provide strength and toughness necessary for cutting.

2.8 Ion milling of curvilinear shapes

A new microfabrication capability has been added to the focused ion beam system. This includes software that allows for sputtering of prespecified '3-dimensional' shapes.(Xie and Vasile) In the past, focused ion beam sputtering has been restricted to milling of rectilinear or prismatic cross-sections. Potentially the ability to fabricate curved features will allow for more geometrically-complex micro-cutting tools and features required in complex, microelectromechanical devices.

The code allows the user to sputter curvilinear shapes including sinusoids, hemispheres and parabolas of different sizes and symmetry. This is accomplished by numerically solving for the

beam pixel dwell times required to sputter a shape of a given depth. The calculation of ion dose required at each pixel within the targeted area accounts for the sputter yield dependence on incidence angle, the sputter yield dependence on material properties and the ion beam intensity distribution. The creation of curved surfaces in initially planar substrates can consist of a large range of incidence angle depending on the depth and net shape. In general, each target material has different sputter yield dependencies.

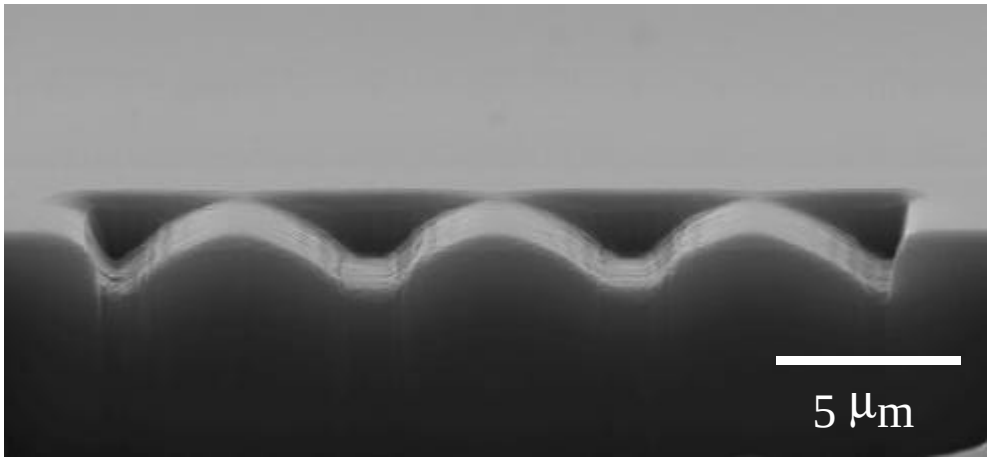

Figure 2.11. Sinusoidal features ion milled into planar Si(100) wafer. Sample was cross-sectioned after 3-d ion milling.

Tests of the 3-d ion milling code consist of sputtering a variety of shapes into polished, planar, single crystal Si(100) substrates. Sputtering of single crystal material is chosen for initial tests to avoid additional effects of crystal texture and compositional variations on sputter yield. Figure 2.11. shows an example of a sinusoid shape sputtered into silicon.

Summary

This work successfully extends conventional milling/turning techniques to the microscale in order to fabricate complex features in a variety of materials. Focused ion beam sputtering is used to fabricate micro cutting tools that have well defined tool geometries. Tools have cutting edge radii of curvature equal to 0.1 μm, although sharper edges may be possible with other tool materials. Focused ion beam tool sputtering has the advantage that almost any conceivable tool geometry can be fabricated on a scale that is well below those reached by grinding methods.

Sharp micro-end mill tools have been made by focused ion beam sputtering. These tools machine ~ 25 μm wide features in different metal alloys. Accurate placement of facets on tools and a proper stage rotation sequence between ion sputter steps is used to make micro-end mills having different numbers of cutting edges. Ultra-precision machining tests with FIB-shaped tools fabricate millimeter long trenches. Trenches have nearly vertical sidewalls and small bottom surface roughness. A good matching of tool diameter to trench width is found for all

materials tested including PMMA, 6061 Al, 4340 steel and brass. This includes machining at table feed rates up to 50 mm/minute.

In addition, this study has fabricated and tested several types of microthreading/ micro-grooving tools. These successfully machine helices in cylindrical workpieces. Feature cross-section closely matches tool shape when machining PMMA, Macor and aluminum alloy. These results suggest that other microtools, for example those having nonorthogonal cutting edges, can accurately fabricate beveled grooves with a given desired cross-section.

References:

1. See for example, Minitool, Inc., Los Gatos, CA, USA.
2. Vasile MJ, Biddick C, and Schwalm SA, Microfabrication by ion milling: The lathe technique, *J. Vac. Sci. Technol. B*, 1994*;* 12, 2388.
3. Harriott LR, A second generation focused ion beam micromachining system, *Proc. SPIE*, 1987; 773, 190.
4. Vasile MJ, Friedrich CR, Kikkeri B, and McElhannon R, Micrometer-scale machining: tool fabrication and initial results, *Precision Engineering*, 1996; 19 (2/3), 180-186. Friedrich CR and Vasile MJ, Development of the micromilling process for high aspect ratio microstructures, *J. Microelectromech. Sys.*, 1996; 5, 33-38.
5. Vasile MJ, Nassar R, Niu Z, Zhang W, and Liu S, Focused ion beam milling: depth control for three-dimensional microfabrication, *J. Vac. Sci. Technol. B*, 1997; 15, 2350-2354.
6. Vasile MJ, Nassar R, Xie J, and Guo H, Microfabrication techniques using focused ion beams and emergent applications, *Micron*, 1999; 30, 235-244.
7. The second apparatus was a joint project among Louisiana Tech University (IfM), the National Jet Company and Dover Instruments.
8. Hardness values for the different metal alloy workpiece materials include 6061-T4 aluminum, Rockwell B =26; brass, Rockwell B = 35; 4340 steel, Rockwell B = 97
9. D.P. Adams, M.J. Vasile, G. Benavides, and A.N. Campbell, Micromilling of metal alloys with focused ion beam-fabricated tools, *Precision Engineering*, 2001, 25, 107-113.
10. D.P. Adams, M.J. Vasile, and A.S.M. Krishnan, Microgrooving and microthreading tools for fabricating curvilinear features, Precision Engineering, 2000, 24, 347-356.

Intentionally Left Blank.

3.0 Laser Machining

The key issue of using lasers for micro-machining is to minimize the heat affected zone (HAZ) surrounding the ablated micro-feature. Because a huge amount of energy is deposited at the machined area on the work-piece, a large melting zone can be created due to the thermal diffusion. Such an effect significantly reduces the precision and accuracy required for the micro-machining operation. To minimize this detrimental effect, two approaches were identified and used in this study. The first approach is to minimize the penetration depth by using a short wave length laser. This can be achieved by excimer lasers (XeC, KrF, and ArF with wave lengths that vary from 308 nm to 192 nm) where most energy can only be absorbed near to the surface[1]. The second approach is to use an ultra-short pulse laser, such as a femto-second laser, where the time scale is too short for the thermal energy to be transferred from the fast electron cooling to the crystalline lattice.[2] Since both mechanisms only permit a short thermal diffusion length, the ablation process is more efficient and material can be precisely removed layer-by-layer. Figure 3.1 illustrates this removal operation on alumina by an excimer laser where the machining depth is linearly proportional to the number of laser pulses. A similar phenomenon is also observed by femto-second laser ablation where each pulse creates a groove-like appearance on the drilling wall of a 5 mil kovar sheet (see Figure 3.2). This layer-by-layer ablation provides a precision control of drilling depth and creates a unique capability to machine three dimensional micro-features.

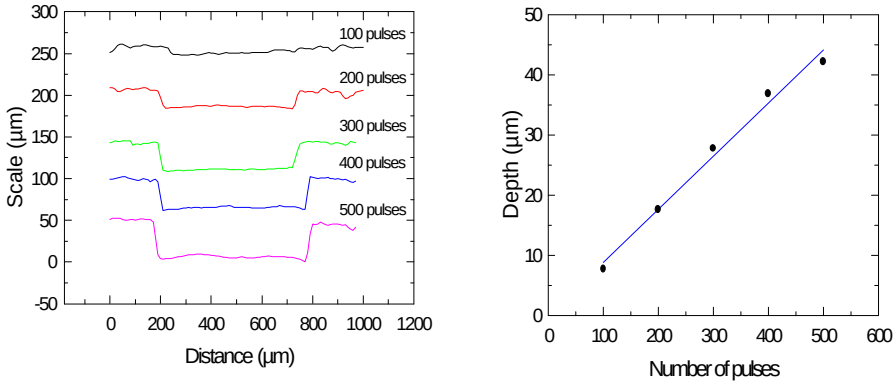

Figure 3.1: (a) The cross-section profiles of excimer laser (KrF) machining on alumina, (b) The number of laser pulses verses the machining depth.

Sandia has an excimer laser (Lumonics Hyperex-400, 248nm) set up for meso-scale machining. The excimer laser machines material by pulsing it with nanosecond pulses (10-25 ns) of ultraviolet light. The workpiece is mounted to precision translational stages which is controlled by a CAD/CAM system. A controller coordinates the motion of the workpiece relative to the stationary UV laser beam and coordinates the firing of the pulses. Figure 3.3 is a schematic setup for a mask projection technique that is used to define machining geometries. The mask is inserted into the excimer laser beam where the fluence is too low to ablate the mask. The pattern geometry on the mask is de-magnified through the lens and projected onto

the work piece. An internal aperture is introduced to reduce the beam divergence which in turn effectively reduces the spot size and enhances the edge definition of a projected image. This approach can be used to machine multiple holes simultaneously. Figure 3.4 is an image of an array of 48 micron holes simultaneously machined into alumina.

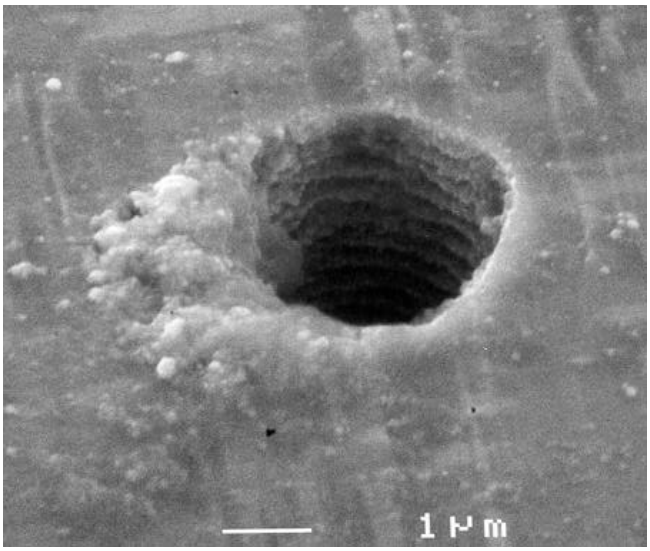

Figure 3.2: A Micro-hole (~3.2 μm) machined in kovar using a Ti-sapphire femto-second laser. Each pulse removes about 0.2 μm of kovar layer.

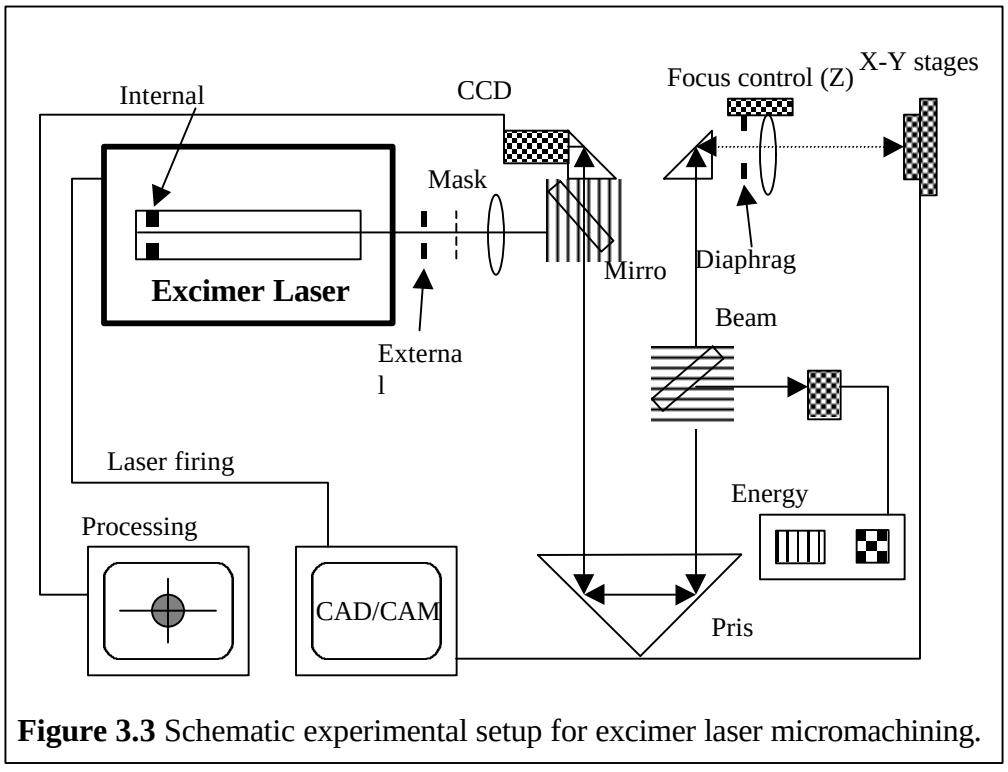

Figure 3.3 Schematic experimental setup for excimer laser micromachining.

Sandia's excimer laser has been used to machine polymers, ceramics, glass, and metals. The general ablation behavior of ceramic, metal, and glass is given in Figure 3.5. For alumina (Figure 3.5 (a)) and stainless steel (Figure 3.5 (b)), the ablation rate quickly increases after passing the ablation threshold, then ablation rate remains constant as fluence increases. The energy density for machining operation is selected at the lowest fluence level where the ablation rate holds constant. This gives a reproducible result without stressing the laser system. When a modern excimer laser system is used where the repetition rate can reach up to 2000 pulses per second, it is possible to achieve an ablation rate of 40,000 cubic microns per second. In contrast to the above materials, the ablation rate of a PZT (lead zirconate titanate) ceramic and a lead glass increases drastically after passing the ablation threshold then decreases as the fluence increases (Figure 3.5 (c)). It is believed that the electron density for the plasmas created over the glass or PZT ceramic during laser processing is greater than 1.8 X 10^{28} m^{-3} (at wavelenght =248 nm).[3] Under such circumstance, the reflection and scattering increases with the laser fluence, thus the incident radiation is significantly attenuated through the plasma.[3] Consequently, the ablation rate decreases. The ablation thresholds and the material removal rates for various materials are summarized in Table 3.1. Figure 3.6 (a) and (b) shows the microphotographs of a 25 micron by 25 micron channel machined by the excimer laser into alumina and PZT ceramics. The vertical walls in the channel are a result of good coupling.of the UV wavelength (248 nm) to the ceramic materials.

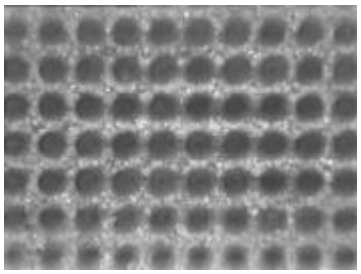

Figure 3.4: An array of 48 micron holes machined into 275 micron thick alumina using excimer laser mask projection (24 mJ/pulse at 30 Hz in air).

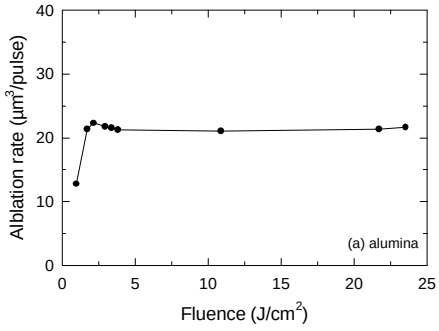

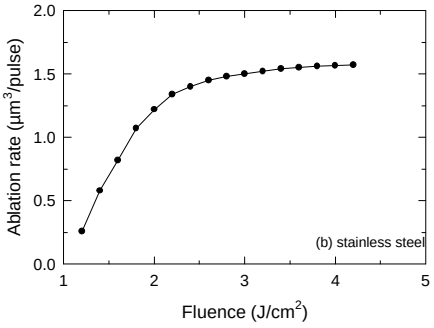

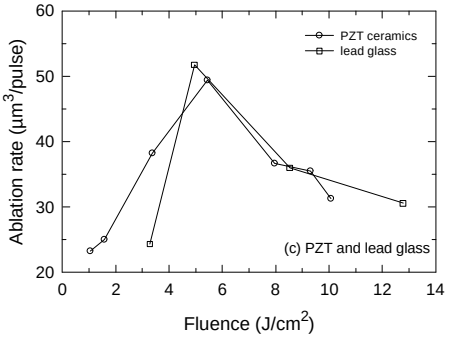

Figure 3.5: The ablation rates for (a) alumina ,(b) stainless steel, (c) PZT and lead glass in air (KrF, 248 nm).

Both excimer laser and femto-second laser machining seem to be capable of ablating various materials. However, it is found in general when the aspect ratio of a micro-feature is large it is difficult to obtain a vertical wall. This is especially true when drilling holes with a tightly focused laser beam. In this case, as the aspect ratio of the depth (t) to the diameter of the focus spot (D) increases, the drilling angle along the walls becomes far from vertical. Consequently, the run-off angle (or the tapered angle) increases as the aspect ratio of the micro-hole increases. Figure 3.7 shows the change of the run-off angle as a function of the aspect ratio of microholes machined on a thin alumina substrate. Preliminary results also indicate that the change of the run-off angle seems to be dependent on the ablation rate of the material, which are consistent with an experimental observation reported in the literature.[4]

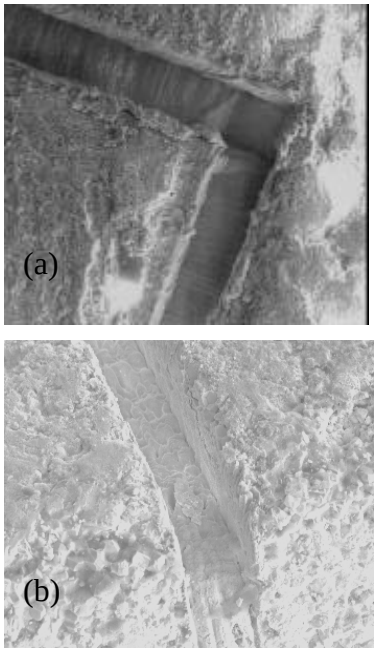

Figure 3.6: 25 μm wide x 25 μm deep trench in (a) alumina (b) PZT using excimer laser.

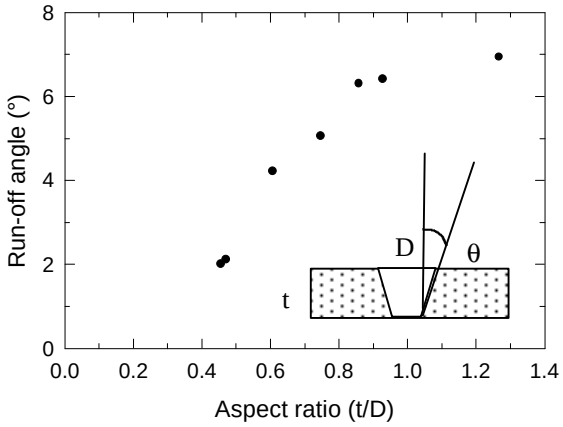

Figure 3.7: The effect of aspect ratio of a microhole on the run-off angle (theta). Data obtained from ablation of alumina in air with a KrF excimer laser.

Another issue associated with micro-machining of small features (< 30 microns) in metals with excimer lasers is the thermal debris build up around focused spot. Figure 3.8 (a) is an image of a 12 micron hole machined by the excimer into kovar using the mask projection technique. The debris on the entrance side of the kovar sheet is a result of thermal melting of the material. Although smaller holes (less than 6 μm) can also be achieved by a higher de-magnification (1/12X), a large, undesired debris

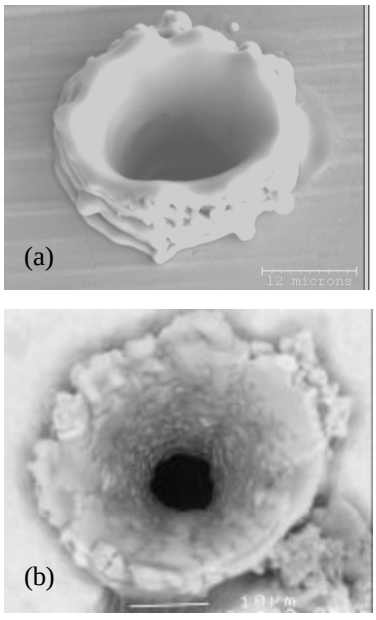

Figure 3.8: (a) 12 μm dia hole x 25 μm deep and (b) 4 to 6 μm hole x 125 μm deep in kovar using excimer laser (KrF, 248 nm)

build-up is created around the focused spot (see Figure 3.8 (b)). As mentioned earlier in this section, the thermal melting and the debris formation are detrimental to meet the demand of high precision required for micromachining. The mask projection technique has been used successfully with a Q-switched YAG lasers as well, however, re-solidified thermal debris is still problematic.

A cleaner laser machining approach is to use a Ti-sapphire femtosecond laser (pulse width on the order of 10^{-15} seconds). Since each laser pulse is less than one picosecond, the energy introduced by laser can not be effectively diffused into the workpiece.[2] As a result, the efficiency of the machining process is very high. Figure 3.9 shows two images of laser machined holes into identical sheets of kovar[5], each hole having a similar diameter. These holes were machined with the Ti sapphire femtosecond laser. The hole shown in Figure 3.9 (b), which was machined in air, is about as clean as the hole in Figure 3.9 (a), which was machined in a vacuum. The detectable debris that can be observed in these images are nano-size particles. The minimal debris resulting from femtosecond machining has also been observed by the University of Nebraska (see Figure 3.10). This microphotograph is also an illustration of a deep one micron-size feature (with extremely high aspect ratio) that can be fabricated using the femtosecond laser.

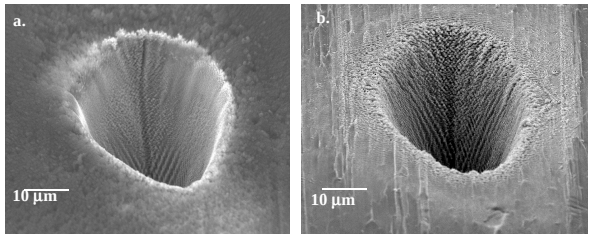

Figure 3.9: Collaboration with Pulsed Power (SNL): Micro-holes machined in kovar using a Ti:sapphire system (120 femtoseconds) in air (a.) and in vacuum (b.). These are compared with a hole. All images are taken from the entry side of the foil.

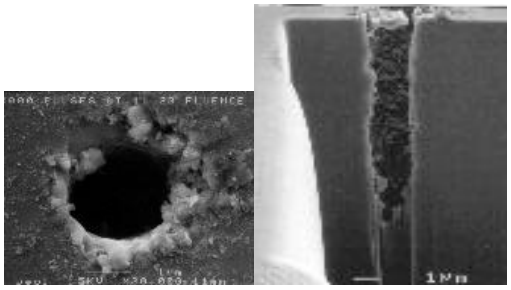

Figure 3.10: Top view and cross-sectional view of 1 µm dia hole in Silicon . Aspect ratio: 10 to 1. (**University of Nebraska, Center for Electro-Optics)**

In summary, femtosecond lasers with ultra-short pulses deliver incredible intensity levels, which can easily reach the hundreds of Terawatts per square centimeter range at the focus spot. No materials can withstand the forces at work at these power intensities, therefore, the ablation process is clean and not material specific. Even for transparent materials, such as quartz, the immense power density of the laser beam can still ablate away these materials through a multiphonon absorption process.[6,7] Despite some intrinsic limitations such as poor beam quality, toxic gas handling, and power stability of the system, excimer lasers have shown versatility of machining various materials. The process creates clean and well defined patterns in ceramics, glass and polymers; however, thermal debris created by nano-second pulses widths, metal might create limitions for machining micro-size features in metals. These results

indicate that short pulse lasers (in the range of sub-picosecond range ($<10^{-12}$ second)) are required for patterning of high thermally conducting materials in order to obtain high precision and minimize thermal damage.

Table 3.1 Ablation Rate for Ceramics,Glass, and Metals. (by KrF excimer laser)

Material	Threshold fluence (J/cm^2)	Ablation Rate (μm^3/pulse)
Alumina	1.0	22.0 @ fluence> 4.0 J/cm^2
Alumina Nittide	1.2	20.0 @ fluence >7.5 J/cm^2
PZT (95/5)	1.0	48.0 @ fluence 4.5 $J/cm^{2\dagger}$
Lead Glass	3.2	54.0 @ fluence 5.5 $J/cm^{2\dagger}$
Stainless Steel	0.3	1.6 @ fluence >3.5 J/cm^2
Kovar	0.7	1.2 @ fluence > 2.8 J/cm^2

† at the maximum ablation rate.

Reference:

1. W. W. Duley, UV Lasers: Effects and Application in Materials Science, Cambridge University Press, Cambridge, UK (1996).
2. B. N Chichkov, C. Momma, S. Nolte, F. von Alvenseben, and A. Tunnermann, " Femtosecond, Picosecond and Nanosecond Laser Ablation of Solids," Appl. Phys. A, **63**, 109 (1996).
3. R. Poprawe, E. Beyer, and F. Herziger, Inst. Phys. Conf. Ser., **72**, 87 (1984).
4. M. Eyett and D. Bauerle, "Influence of Beam Spot Size on Ablation Rates in Pulsed-Laser Processing", Appl. Phys. Lett, **51**, (24), 2054 (1987).
5. D. E. Bliss, D. P. Adams, S. M. Cameron, and T. S. Luk, "Laser Machining with Ultrashort Pulses: Effects of Pulse-Width, Frequency and Energy," Material Science of Microelectromechanical Systems (MEMS) Devices, Mat. Res. Soc. Symp. Proc., Vol 546 (1999).
6. J. Ihlemann, B. Wolff, and P. Simon, "Nanosecond and Femtosecond Excimer Laser ablation of Fused Silica", Appl. Phys. A, 54, 363 (1992).
7. H. Varel, D. Ashkenasi, A. Rosenfeld, M. Wahmer, and E. E. B. Campbell," Micromachining of Quartz with Ultrashort Laser Pulses," Appl. Phys. A., 65, 367 (1997).

4.0 **Micro-EDM (electro-discharge machining)**

Electro-discharge machining removes material through a spark erosion process. The micro-EDM machines can machine features as small as 25 microns because the micro-generator needed to create the spark has the necessary fine control to minimize the energy per pulse for the smaller features. These low energy pulses sent in rapid succession not only produce smaller features but also minimize the surface roughness to about 0.1 microns Ra. For either the sinker or the wire micro-EDM machine, the two major considerations for determining feature size are the electrode size and the over-burn gap. Sandia has used electrodes as small as 25 microns in diameter and over-burn as little as 3 microns. Currently, Sandia has an Agie Compact 1, micro-sinker EDM machine (see figure 4.1) and an Agie Excellence 2F micro-capable wire EDM machine (see figure 4.2). The advantage to the sinker EDM process is that an electrode having a complex three-dimensional geometry can be sunk into a work piece creating the conformal geometry in the work piece. A disadvantage to the sinker EDM is that the electrode also erodes during the EDM process (although at a much slower rate). Vertical side-walls are more difficult with the sinker EDM process due to electrode wear. The advantage to the wire EDM process is that unused wire can be circulated to the work piece during the EDM process thereby presenting to the work piece an electrode having a known geometry. The disadvantage to the wire EDM process is that the feature cuts are usually of a simpler geometry (two and a half dimensional). Although, the Agie Excellence 2F wire machine can make a somewhat more complex cut because of its ability to tilt the wire (4^{th} axis capable).

Creating an electrode having a complex geometry for the sinker EDM machine is not trivial. Graphite is a very desirable electrode material because it machines easily and it erodes slowly (i.e., the work piece erodes quickly but the electrode maintains its shape longer). Also, hundreds of complex finely featured graphite electrodes can be fabricated from one master die by way of ultrasonic grinding. Features as small as 50 microns can be ultrasonically ground into high density finely grained graphite. Copper is also very common electrode material. Another approach to fabricating a complicated sinker micro EDM electrode for a meso-scale part is to use the LIGA process. LIGA is a lithographic process that additively builds meso-scale parts by electroplating material into molds. Copper, which is a good performing electrode material, can be plated into LIGA molds. The copper LIGA fabricated electrode can then be mounted onto the sinker micro-EDM machine to fabricate a part in yet a different material such as stainless steel or kovar. This hybrid process is a method of extending the material base for LIGA.

Figure 4.3 is an image of a small intricate copper electrode fabricated by the LIGA process. This electrode was then used to EDM through a .006 inch thick kovar sheet. If the electrode can be described as the bricks then the machined work piece would be the “mortar” that fits between the bricks. Figures 4.4 and 4.5 respectively show the entrance side and the exit side of the kovar part. The most challenging feature on the kovar part is the portion of the “mortar” that is .002 inch thick by .006 inch deep (measured into the page). A parametric study was performed to determine the optimal over burn gap that yields an acceptable part

Figure 4.1: Agie Compact 1, micro-sinker EDM machine.

Figure 4.2: Agie Excellence 2F micro capable wire EDM machine.

Figure 4.3: Micro-EDM electrode in copper made with the LIGA process.

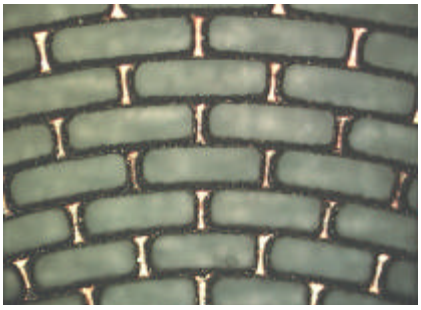

Figure 4.4: Entrance side of kovar part.

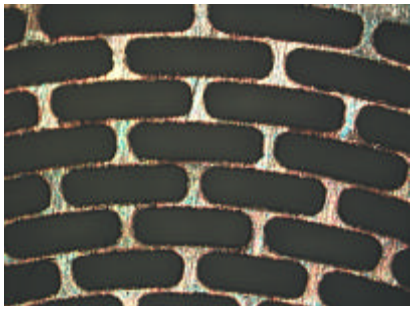

Figure 4.5: Exit side of kovar part.

machined within a reasonable time. A relationship exists between the over-burn gap and the machining time. The smaller the over-burn gap the finer the features but the greater the time required to machine the part. The kovar part was machined with copper electrodes having an over-burn gap of .0005 inch, .001 inch, .0015 inch, and .002 inch. The over-burn gap parameter can easily be varied by under sizing the LIGA fabricated electrode to the corresponding gap. The .0015 inch over-burn gap was a compromise which resulted in a good part that was machined in about 15 minutes.

Both graphite and copper are good electrode materials but for different reasons. Desirable electrodes maintain their shape longer and therefore do not need to be replaced as often for a fresh electrode when machining multiple parts. Material properties for a desirable electrode include high heat conductivity, high specific heat, and high melting point. Graphite obviously excels in regards to melting point while copper readily conducts heat. The ultrasonically ground graphite electrode produced a part similar to that shown in figures 4.4 and 4.5, however, the graphite electrode maintained its shape better than copper.

The micro-EDM process enables the fabrication of meso-scale parts in difficult to machine conductive materials such as tungsten, diamond, hardened tool steel, doped silicon, gallium arsenide, and rare earth magnetic materials. Figures 4.6, 4.7, and 4.8 illustrate a 6 degree stepper motor that was enabled by micro-EDM. This stepper motor is a pancake style motor (10mm x 10mm x 5mm) designed for high torque, low speed applications. This style of motor is suitable for direct drive applications thereby eliminating the need for gear reduction subassemblies. High performance motor materials must be used to maximize the power output per unit volume of motor. The difficult to machine, high performance materials used for this motor include Hiperco alloy and Neodymium iron boron. The rotor material is neodymium iron boron and the stator material is Hiperco alloy. This motor was assembled and successfully operated.

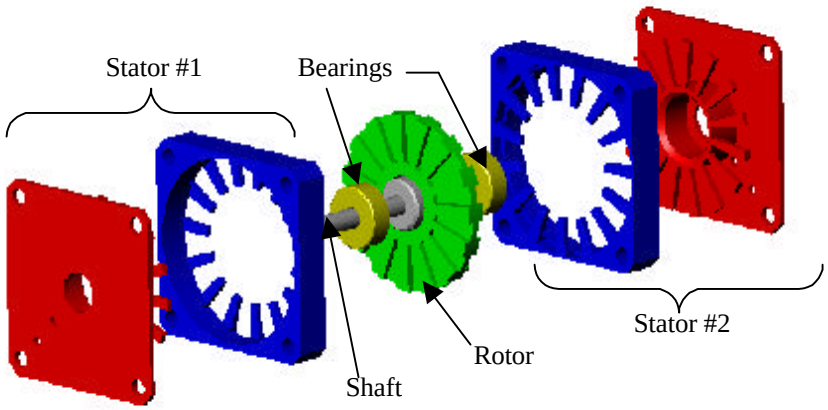

Figure 4.6: Exploded solid model of 10mm x 10mm x 5mm stepper motor.

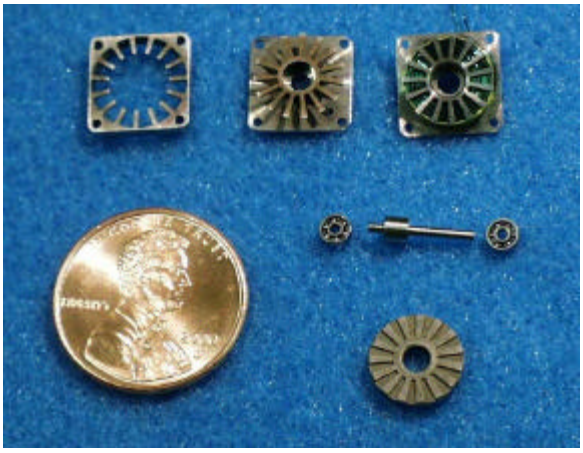

Figure 4.7: Stepper motor piece parts.

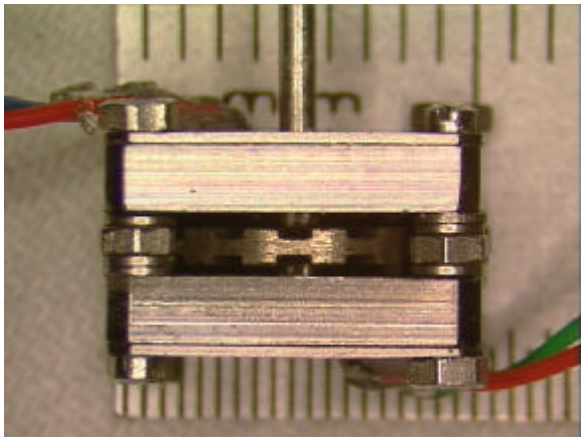

Figure 4.8: Assembled stepper motor.

The important parameters for EDM in general include, pulse energy, pulse rate, polarity, electrode material, dielectric fluid, over-burn gap, and flushing. The pulse energy has its own set of parameters such as voltage, current, and pulse duration. The pulse energy controls the size of crater eroded from the work piece. The pulse rate is a major factor that controls how quickly material is removed. The pulse rate must allow for sufficient time between pulses so that the dielectric fluid has time to recover (i.e. de-ionize) and for particles to be flushed away. The polarity which defines whether the electrode is the cathode or anode can greatly affect the relative erosion rate of the electrode versus the work piece (i.e., electrode wear). The over-burn gap is a dependent parameter that can be controlled by varying the voltage/current profile during a pulse. A smaller over-burn gap requires a smaller breakdown voltage. An important consideration that is sometimes difficult to implement for the micro EDM process, is flushing. Particles that are being generated during the EDM process need to be flushed away from the over-burn gap region. These particles can quickly accumulate and create an electrical short between the electrode and the work piece. Particles are typically flushed away by circulating the dielectric fluid through the over-burn gap region. For over-burn gaps as small as 3 microns, it is sometimes difficult to flush the particles away. The flushing problem is more prominent in regards to the sinker micro-EDM process rather than the wire micro-EDM.

Reference:

1. J.P. Kruth, F. Staelens, “Non-traditional Machining Methods, Electro-Discharge Machining”, Katholieke Universiteit Leuven, 1993-1994.
2. H.C. Moser, B. Boehmert, “Trends in EDM”, Modern Machine Shop Feb. 2000
3. K. Takahata, N. Shibaike, H. Guckel, “High-aspect-ratio WC-Co microstruture produced by the combination of LIGA and micro-EDM”, Microsystems Technologies 6 (2000) 175-178.

5.0 SUMMARY OF CAPABILITIES

As in the macro world, no one meso-scale machining process can do it all. Some meso-scale processes are more encompassing than others, but each process has its niche. As in the macro world, designers usually require a variety of materials to optimize performance of mechanical components. For example hermeticity and corrosion resistance may be important characteristics for housing (or packaging) materials but wear and friction characteristics may be important for gears internal to the housing. Gears and housings made from non-magnetic materials are desirable when used in the vicinity of electromagnetic actuators. **Table 5.1** is an attempt by the authors to summarize meso-machining processes. The data in the table is meant to be a representation of the technology but does not represent any particular machine manufacturer. The first column in the table lists the technology and also whether the technology can fabricate 3D features or 2D (actually 2.5D) features only. The second column indicates minimum feature size and the tolerance associated with that feature. For example the minimum feature size for micro-milling is 25 microns channel plus or minus 2 microns. The source for the tolerance assigned to micro-milling is a result of the radial run out of the tool when mounted in the collet. The third column lists the feature positional tolerance, which is mostly based upon the quality of positional stages used on the machine, however, work piece set-up accuracy also plays a role. In the example of micro-milling, the 25 micron channel can be positioned on the work piece to plus or minus 3 microns. The fourth column lists the material removal rate, which is an indicator of how quickly parts can be machined. The FIB has a very poor material removal rate, which was a driver for using the FIB to fabricate micro-tools. Although it can take a long time to make a micro-tool, the micro-tool has a high material removal rate and can be used for a significant duration (up to six hours). A feature tolerance and feature positional tolerance of about 3 microns does not compare favorably with LIGA. Nevertheless, a 3 micron profile tolerance on ratchet teeth (for example) on a 6 mm diameter part is an equivalent ratio to a .001 inch profile tolerance on a 2 inch diameter part. The point is, 3 microns is probably plenty good enough.

Meso-machining processes can create true three dimensional piece parts. As an example, a single part can be fabricated having a gear, hub, and shaft. The meso-machining process can eliminate the need to assemble a shaft and hub to the gear which is a difficult assembly. Press fits for meso-scale parts requires only microns of interference. Meso-machining can eliminate the need to press fit a shaft. Meso-machining processes offer the best relative tolerance capabilities for precision parts (i.e., the tolerance of the dimension, normalized by the dimension). The relative tolerance capability of silicon based MEMS processes is about equivalent to the relative tolerances used to build a house.

Technology / *Feature Geometry*	**Minimum feature size / *Feature tolerance***	**Feature positional tolerance**	**Material removal rate**	**Materials**
Focused Ion Beam / *2D & 3D*	200 nanometers / *20 nanometers*	100 nanometers	.5 cubic microns/sec	Any
Micro milling or micro turning / *2D or 3D*	25 microns / *2 microns*	3 microns	10,400 cubic microns/sec	PMMA, Aluminum, Brass, mild steel
Excimer laser / *2D or 3D*	6 microns / *submicron*	submicron	40,000 cubic microns/sec	Polymers, ceramics and metals to a lesser degree
Femto-second laser / *2D or 3D*	1 micron / *submicron*	submicron	13,000 cubic microns/sec	Any
Micro-EDM (Sinker or Wire) / *2D or 3D*	25 microns / *3 microns*	3 microns	25 million cubic microns/sec	Conductive materials
LIGA / *2D*	submicron / *0.02um~ 0.5 um*	~0.3um nom. across 3"	N/A	Electroformable: copper, nickel, permalloy (see note)
Note: LIGA can also be used to fabricate parts in polymers, pressed powders, ceramics, and rare-earth magnets with a little degradation in machining performance specifications.				

Table 5.1: Comparison of meso-machining processes.

References:

1. Marc Madou, “Precision Machining Applications Domain”, Fundamentals of Microfabrication, CRC Press, 1997

2. "Nanotribology: Critical Assessments and research needs", edited by S. M. Hsu, Kluwer Academic Press, Boston, MA, USA, to be published in Oct. 2000.

6.0 ISSUES

Designers are comfortable with traditional materials (e.g. stainless steel) because these materials have a long history and have been very well characterized through the years. Meso-scale machining processes allow the designer to use traditional materials. On the other hand, tribological issues for meso-scale parts may or may not emulate what is already known. Subtractive meso-scale machining technologies expand the material base and increase the combinations of materials that can come into contact. Galling may be an issue with some material combinations. Each particular meso-scale machining process uniquely affects the surface roughness and morphology. Micro-milling and micro-turning may generate burrs and particles that can cause mechanical interference. Micro-EDM may leave a recast layer that can have either favorable or unfavorable wear and friction characteristics. Friction effects of meso-scale parts sliding with other parts may have limited points of contact and are not accurately modeled by surface contact models. Some meso-scale machining technologies, such as micro-EDM, are fairly mature, while others, such as femtosecond laser machining, require additional development. Material stability may be of greater concern for high precision, low aspect ratio parts. For example, a very thin gear may warp like a potato chip upon being machined if the material stress relieves. A number of stable non-magnetic materials are being considered for meso-scale parts, such as, Nitronic 60 stainless steel, Titanium, and Beryllium Copper. Machine tool forces are a non-issue for meso-machining processes such as femtosecond laser machining and micro-EDM and therefore do not contribute to the deformation of meso-scale parts. Many issues have yet to be identified.

Intentionally Left Blank.

Distribution:

5	MS 0958	Gil Benavides, 14184
5	MS 0959	Pin Yang, 14192
5	MS 0959	David Adams, 14171
1	MS 0319	Charles Vanecek, 2613
1	MS 0960	Norm DeMeza, 14100
1	MS 0961	Carol Adkins, 14101
1	MS 0188	LDRD Office, Attn: Donna Chavez
1	MS 9018	Central Technical Files, 8945-1
2	MS 0899	Technical Library, 9616
1	MS 0612	Review & Approval Desk, 9612 (for DOE/OSTI)